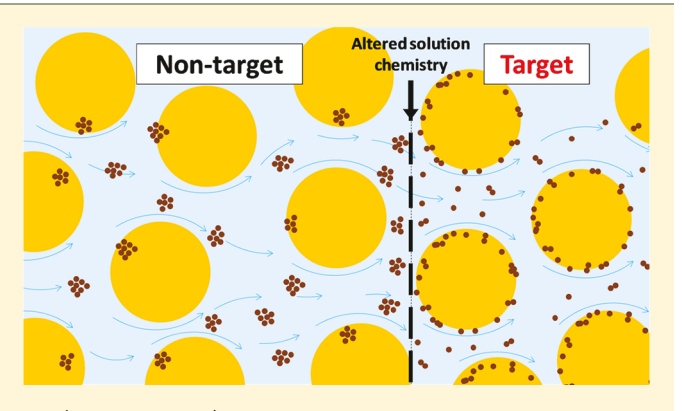


# Theory-Guided Targeted Delivery of Nanoparticles in Advective **Environmental Porous Media**

Cesar A. Ron, Mei Dong, Saren L. Wooley, and William P. Johnson, Johnson

Supporting Information

ABSTRACT: For near-neutrally buoyant colloids, retention on surfaces is dramatically reduced for radii in the range from approximately 100 nm to 1  $\mu$ m (i.e., n- $\mu$  transition) under unfavorable conditions (energy barrier present). Given that unfavorable conditions are predominant in the environment, the above-described characteristic is underutilized in strategies for targeted delivery of nano- to microscale particles (colloids) in porous media. We present herein, a strategy that involves tuning colloid size within the  $n-\mu$  transition range to minimize retention in non-target porous media, followed by solution chemistry-triggered disaggregation to yield nanoscale colloids and promote retention in target porous media. Toward this purpose we examined the transport properties of aggregated



and disaggregated carboxylate-modified latex (CML) nanospheres (55 nm radius) and novel shell cross-linked knedel-like (SCK) nanoparticles (10-50 nm radius). Colloid retention was measured on soda-lime glass (silica) in an impinging jet system representing upstream sides of porous media grains. Continuum scale attachment rate coefficients  $(k_f)$  were determined from the experimental colloid retention and were then utilized to predict the distribution of retained colloids from source in target porous media at field scales. These experiments and simulations demonstrate the viability of size-tuning colloids to the  $n-\mu$ transition range in order to facilitate their transport through non-target porous media. Disaggregation triggered by, for example, reduced ionic strength achieved by preferential advection of colloids, was demonstrated to greatly increase retention in target porous media, with an expectation of increased surface area and enhanced reactivity.

### INTRODUCTION

Targeted delivery of novel nano- and microparticles (herein referred to as colloids) in porous media is a major aspect of remediation of subsurface contamination. A primary motivator for targeted delivery is the need to minimize loss of colloids in non-target porous media, including cases where the goal is to avoid clogging the area of injection, 1-4 as well as cases where the target media is not accessible to direct injection (e.g., beneath a permanent structure).

A size-based transport-triggered strategy for targeted delivery of humic acid-stabilized (HA) iron oxide goethite (FeO<sub>x</sub>) nanoparticles (NPs) (~50 nm radius) in environmentally relevant media (quartz sand) was recently demonstrated. After arrival at the target location, HA-FeO, NPs were immobilized by aggregation through cation bridging with Ca<sup>2+</sup>. This aggregation was triggered by faster advection of the HA-FeO<sub>x</sub> NPs relative to a leading Ca<sup>2+</sup> solution that was previously injected. That colloids can transport faster than solutes in groundwater is a well-recognized phenomenon that arises from their lower diffusion into low-advective zones relative to solutes. While this property is most clearly recognized in fractured media,6 the differential advection of colloids relative to a solute is well recognized in a variety of granular media.<sup>7-12</sup> HA-FeO<sub>x</sub> NPs were destabilized where they reached the leading Ca2+ solution.5

Delivery of novel colloids for enhanced in situ subsurface contaminant degradation is a common goal for both  $metallic^1$  and carbonaceous colloids.  $^{13-17}$  Because pore size and fluid velocity are often unalterable in a given environmental context, colloid size is often the primary parameter to optimize. Colloid size is often misunderstood to favor greater transport of smaller colloids. However, the physics of mass transport underlying colloid filtration theory (CFT)<sup>18,19</sup> dictates that delivery to grain surfaces in porous media (quantified as collector efficiency,  $\eta$ ) is least for the size range with the lowest combined diffusion and sedimentation. For near-neutrally buoyant colloids under typical groundwater velocities, this range is from approximately 100 nm to 1.0  $\mu$ m (radius), which we refer to as the  $n-\mu$  transition.<sup>20</sup>

Received: July 31, 2019 Revised: August 29, 2019 Accepted: August 30, 2019 Published: August 30, 2019

<sup>&</sup>lt;sup>†</sup>Department of Geology & Geophysics, University of Utah, Salt Lake City, Utah 84112, United States

Departments of Chemistry, Materials Science & Engineering, and Chemical Engineering, Texas A&M University, College Station, Texas 77842, United States

Upon delivery to the grain surface, colloid attachment is mediated by multiple forces (electric double layer, van der Waals, and others) acting over contrasting distances that may produce net repulsion (energy barrier) unfavorable to attachment, as considered typical of environmental conditions. Nanoscale charge heterogeneity (e.g., charge and roughness  $^{20,22-27}$ ) on surfaces has long been invoked to explain observed colloid attachment despite unfavorable conditions, wherein colloid attachment is otherwise predicted to be insignificant. Recently, it was demonstrated that the minimum  $\eta$  observed for  $n-\mu$  transition colloids under favorable conditions is exaggerated under unfavorable conditions, and this can be mechanistically explained by colloid interaction with nanoscale heterogeneity on grain surfaces.

This paper describes a strategy for targeted delivery of colloids in porous media that capitalizes on the newly recognized exaggerated minimum retention for  $n-\mu$  transition colloids observed under unfavorable conditions. The strategy involves aggregating nanoparticles to the  $n-\mu$  transition size range in order to minimize their retention in non-target porous media, and then disaggregating them to maximize retention in target porous media, as triggered by altered solution chemistry, e.g., via differential transport of solutes and colloids. We demonstrate this strategy via experimentally observed colloid retention on surfaces, experimentally measured size distributions, and calculated surface interactions, in response to changes in solution chemistry for carboxylate-modified polystyrene latex (CML) nanospheres (55 nm radius). We also demonstrate the relevance of the concept to novel shell cross-linked knedel-like (SCK) polymeric nanoparticles (10-50 nm radius), which were developed to have a high capacity for solubilizing hydrocarbons.<sup>29</sup>

## ■ MATERIALS AND METHODS

**Colloidal Suspensions and Collector Surfaces.** Experiments examined 55 nm radius fluorescent CML ( $\lambda_{\rm ex}$  = 505,  $\lambda_{\rm em}$  = 515 nm) nanospheres (Molecular Probes Inc., Eugene, OR) and shell cross-linked knedel-like (SCK) nanoparticles. These particular SCKs were core—shell nanoparticles composed of a polystyrene hydrophobic core enveloped by a poly(acrylic acid) hydrophilic corona supported by an ethylamine-derived cross-linker (2,2'-(ethylenedioxy)bis(ethylamine)) with a block copolymer structure of polystyrene<sub>182</sub>-block-poly(acrylic acid)<sub>77</sub> (PS<sub>182</sub>-b-PAA<sub>77</sub>)<sup>29</sup> (Figure S13). A detailed description of SCK preparation is provided in the Supporting Information.

Colloid suspensions were prepared as described in the Supporting Information. Hydrodynamic radii and electrophoretic mobilities (EPM) were measured using a  $\zeta$ -potential analyzer (Mobiu $\zeta$ , Wyatt Technology Corp., Santa Barbara, CA) (Table S1).

Soda-lime glass (herein referred to silica) coverslips (Fisher Scientific, Inc.) were used as the collector surface in transport experiments. Cleaning and characterization are described in the Supporting Information.

Impinging Jet Experiments. A custom-made stainless-steel impinging jet flow cell (radially symmetric) (Figure S4) was used to observe attachment, as described in previous studies <sup>24–26,30</sup> as well as in the Supporting Information. Attachment was quantified as a single cell collector efficiency ( $\eta$  = number attached/number injected) <sup>24,25</sup> under both favorable ( $\eta_{\text{fav}}$ ) and unfavorable ( $\eta_{\text{unf}}$ ) conditions. The ratio of unfavorable to favorable attachment was quantified as a collision efficiency ( $\alpha = \eta_{\text{unf}}/\eta_{\text{fav}}$ ).

**Extended DLVO Profiles.** Particle—particle and particle—collector interactions were calculated using sphere—sphere and sphere—plate geometries, respectively. Surface interactions included van der Waals (vdW), electric double layer (EDL), Lewis acid—base (LAB), steric, and Born, as described in previous publications <sup>24,25,30–32</sup> and in the Supporting Information. For SCKs, equations describing vdW interactions for layered systems were derived in order to account for the materials present in SCK cores and coronas (Supporting Information).

Pore-Scale and Macroscale Particle Trajectory Simulations. To translate the impinging jet results to porous media, pore-scale trajectory simulations were performed in a Happel sphere-in-cell collector 18,33 on the basis of a Lagrangian solution of forces and torques acting on the colloid at each time step, 20,24,31 as described in the Supporting Information. Pore-scale trajectory simulations incorporate discrete representative nanoscale heterogeneity (DRNH)<sup>20</sup> and account for the effects of roughness on hydrodynamic slip and colloidcollector interactions, 26 as described in the Supporting Information. The Happel collector efficiencies  $(\eta)$  were determined by matching simulated  $\alpha$  to experimentally observed  $\alpha$  under unfavorable conditions (Supporting Information). Happel  $\eta$  values under unfavorable conditions were then upscaled to produce continuum scale attachment rate coefficients  $(k_f)$  by accounting for the compounded loss of colloids during transport through successive Happel collectors in a series representing a given porous media (e.g., Johnson and Hilpert<sup>34</sup>). Upscaling to  $k_f$  via  $\eta$  was moderated by efficiencies of fast and slow attachment as previously described.35

Values of  $k_{\rm f}$  determined from upscaling of Happel  $\eta$  values were used to predict the distribution of retained colloids with a distance from the source. Transport was predicted using a continuum-scale Lagrangian transport model as described in Johnson et al. to account for distributions of residence times prior to attachment under unfavorable conditions. Another upscaling option accounts for the impact of colloid size distribution on blocking of colloid attachment by previously attached colloids, thich generates transient breakthrough in response to sustained colloid injection. The upscaling utilized here corresponds to a steady-state breakthrough obtained during step injection of the colloids.

# ■ RESULTS AND DISCUSSION

Minimum  $\alpha$  for  $n-\mu$  Transition Colloids in Porous Media. That colloid retention under favorable conditions is lowest for the colloid size range with the least combined diffusion and sedimentation has long been predicted by CFT<sup>18,19</sup> and is corroborated by experimentally observed collector efficiencies ( $\eta$ ) (e.g., Pazmino et al., <sup>24</sup> Rasmuson et al. 25) where  $\eta$  is the ratio of retained colloids relative to all colloids that entered the collector. In CFT, the collector is a solid spherical grain surrounded by a fluid shell<sup>18</sup> that when repeated in series represents a given porous media. More recently, collision efficiencies  $(\alpha)$ , which are the ratios of  $\eta$ values under unfavorable relative to favorable conditions, were shown to yield a minimum for the  $n-\mu$  transition colloid size range, <sup>20</sup> which corresponds to the least combined diffusion and fluid drag, and hence reduced likelihood of finding heterodomains on which to attach.<sup>20</sup>

Whereas the existence of a minimum  $\alpha$  for  $n-\mu$  transition colloids was established in an impinging jet (silica surface), <sup>20</sup>

this characteristic also exists for transport in porous media (e.g., glass beads),<sup>37</sup> as demonstrated by comparison of results from both systems (Figure 1, triangles). The observed

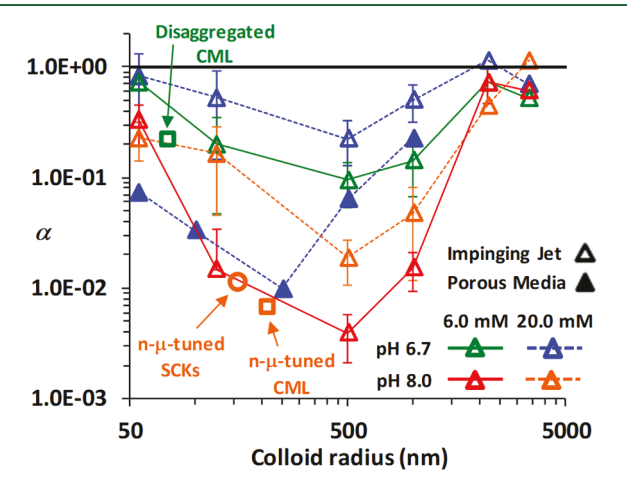


**Figure 1.** Experimental collision efficiencies ( $\alpha$ ) for transport of primary size CML (open triangles),  $^{20}$  n- $\mu$ -tuned and disaggregated CML (open squares), and n- $\mu$ -tuned SCKs (open circles) on silica slides in an impinging jet, and for transport of primary size CML on silica glass beads porous media in a packed column (closed triangles symbols). Solution conditions are as indicated in the legend, and fluid velocities were  $1.7 \times 10^{-3}$  and  $4.6 \times 10^{-3}$  ms<sup>-1</sup> in the impinging jet and porous media, respectively. Primary and disaggregated SCKs were too small for observation via our optical setup. Thus, transport experiments utilized SCKs with high fluorescein labeling, which yielded SCKs primary size distribution in the n- $\mu$  transition range (Figure S3). CML stands for carboxylate-modified latex nanospheres, whereas SCK stands for shell cross-linked knedel-like nanoparticles.

minimum  $\alpha$  for  $n-\mu$  transition colloids decreases with decreased favorability of the colloid–surface interaction, with the most unfavorable interaction (highest pH, lowest ionic strength (IS)) yielding the lowest  $\alpha$ , and vice versa (Figure 1). The order of magnitude lower  $\alpha$  for glass beads (porous

media) relative to the glass slide (impinging jet) is due to the contrasting flow fields in porous media (convergent—divergent) versus impinging jets (divergent only). Whereas the above observation was established using CML, it was also indicated for a wide variety of nonbiological and biological colloids including silica colloids, engineered nanoparticles (ENP), viruses, bacteria, and protozoa, demonstrating that materials of contrasting surface properties (e.g., hydrophobicity, Lewis acid—base) display this behavior.

Tuning Colloid Size within the  $n-\mu$  Transition Range. Under primary conditions (pH 8.0, IS 3.0 mM NaCl) prior to size tuning, DLS measurements demonstrate a narrow size distribution for CML of approximately 55 nm radius (Figure 2b) and for SCKs ranging between 10 and 50 nm (Figure 2c). Calculated colloid—colloid interactions (XDLVO) under primary conditions indicate that the repulsive barrier to aggregation exceeded 10 kT for primary CML (Figure 3a) as well as for primary SCKs (Figure 3c), and both nanoscale colloids lacked attractive primary minima, consistent with their measured stable nanoscale hydrodynamic radii (Figure 2b,c). Because SCKs have core—shell layering, we provide XDLVO formulas for layered systems in the Supporting Information.

To tune colloid size to lie within the  $n-\mu$  transition range, IS was modified with MgCl<sub>2</sub> to achieve 20.0 mM IS (5.6 mM MgCl<sub>2</sub> + 3.0 mM NaCl), which according to XDLVO calculations, eliminated the repulsive barrier to aggregation for both CML (Figure 3a) and SCKs (Figure 3c). The XDLVO calculations indicated the existence of attractive primary minima of approximately -25~kT (CML) and -13~kT (SCKs). Under this condition, CML and SCK sizes increased (Figure 2b,c), yielding aggregate sizes in the  $n-\mu$  transition range with hydrodynamic radii ranging 120-1000 nm (CML) and 115-450 nm (SCKs) according to DLS measurements.

Because our goal was to trigger colloid disaggregation upon reaching the target porous media via altered solution chemistry, we examined the impact of diluting the  $n-\mu$ -tuned colloid solutions by a factor of 10 in pH-equivalent low IS solution to reduce solution IS to 5.0 mM (0.56 MgCl<sub>2</sub> + 3.3

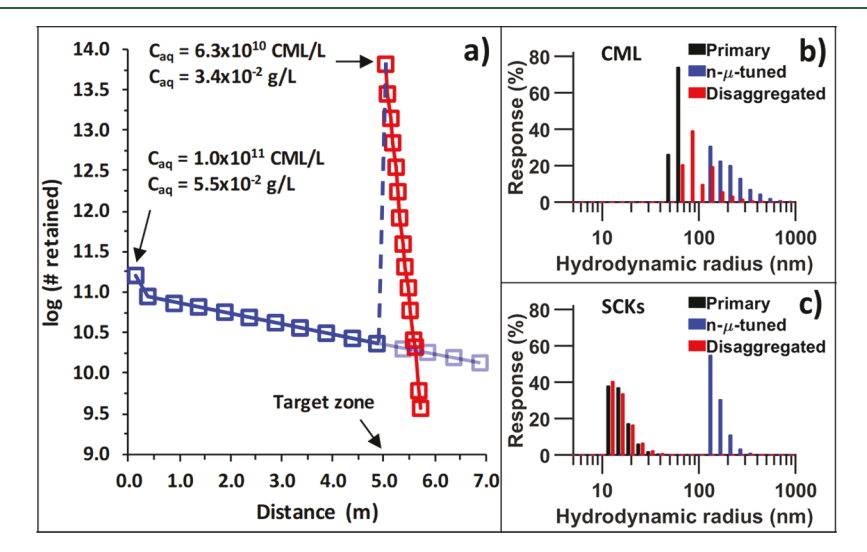


Figure 2. (a) Predicted distribution of retained  $n-\mu$ -tuned CML (blue squares) and disaggregated CML (red squares) in a system composed of medium-grained sand (0.51 mm grains) with porosity of 0.35 and an average pore water velocity of 4 m/day. Transparent squares correspond to predicted distribution of retained  $n-\mu$ -tuned CML if disaggregation is not triggered. Indicated concentrations correspond to CML in the aqueous phase. (b) Number-based dynamic light scattering (DLS) hydrodynamic radius distribution for CML and (c) SCKs. Conditions were pH 8.0 and IS 3.0, 20.0, and 5.0 mM, for primary,  $n-\mu$  tuned, and disaggregated colloids, respectively.

**Environmental Science & Technology Letters** 

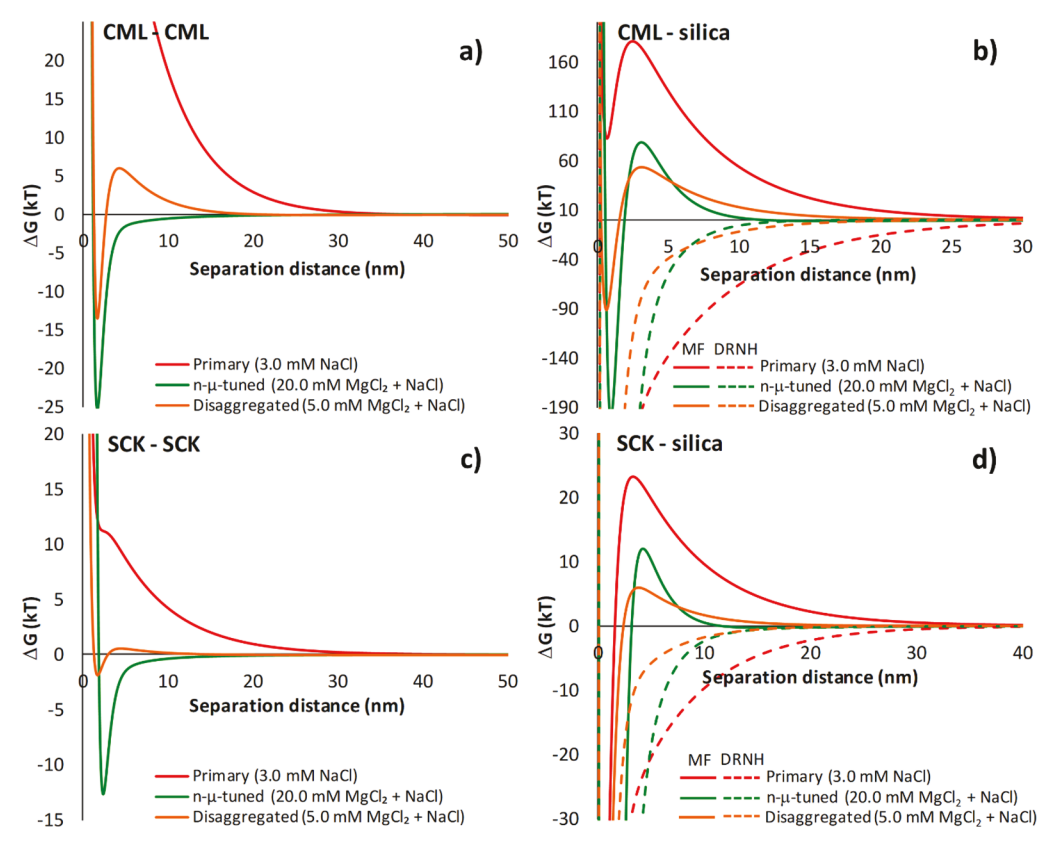


Figure 3. XDLVO energy profiles for (a) CML–CML, (b) CML–silica, (c) SCK–SCK, and (d) SCK–silica surface interactions. Solution conditions were pH 8.0 and IS as described in legend. Solid lines correspond to mean-field (MF) XDLVO interactions. Dashed lines correspond to XDLVO interactions incorporating discrete representative nanoscale heterogeneity (DRNH).

mM NaCl), as may occur via differential advection in targeted delivery. The reduced IS reestablished the repulsive barrier to approximately 5 kT (CML) and 0.6 kT (SCKs) and reduced the depth of the primary minimum to -13~kT (CML) and -2~kT (SCKs) (Figure 3a,c). Disaggregation driven by reduced attraction yielded nanoscale colloid sizes, with mean values at approximately 75 nm (CML) and 16 nm (SCKs) (Figure 2b,c). Notably, the  $\zeta$ -potentials of disaggregated colloids were higher (less negative) than their primary precursors (Table S1), presumably due to remaining Mg<sup>2+</sup> used for aggregation.  $^{38-40}$ 

The kinetics of aggregation and disaggregation to/from the  $n-\mu$  tuned colloid size was examined via repeated DLS. The results demonstrate that  $n-\mu$  tuned CML and  $n-\mu$  tuned SCK were stable within 1 min and remained stable for at least 4 h (duration of preparation and experiment) (Figure S1). Disaggregation yielded a target nanoparticle size within 10 min (Figure S2). In the field, the kinetics of disaggregation will be controlled by mixing between the faster-advancing colloidal and slower-advancing solute (e.g., low IS and/or chelating agent) plumes. The colloidal suspensions utilized in this work were prepared at least 1 h before performing transport experiments to ensure steady state colloid sizes.

Retention of  $n-\mu$ -Tuned Colloids. Retention (on silica) of primary,  $n-\mu$ -tuned, and disaggregated colloids was examined via impinging jet transport experiments. Retention on silica was an order of magnitude lower for  $n-\mu$ -tuned CML relative to their primary components (Figure 1, squares versus triangles), and equivalent-sized CML, as suggested by trends in the data (Figure 1, squares versus dashed line). The greater  $\alpha$  for an equivalent-sized CML relative to a  $n-\mu$  tuned CML

(aggregate) reflects the small radius of curvature (reduced interaction) for primary nanoscale colloids interacting with the surface, as reported for aggregates<sup>41</sup> and asperities on surfaces.<sup>26</sup> Retention was more than a magnitude lower for  $n-\mu$ -tuned SCKs relative to primary CML (Figure 1, circle versus triangles), suggesting that the size tuning strategy is also viable for SCKs. Disaggregated CML were retained on silica similarly to primary CML, both of which were retained by an order of magnitude greater than for  $n-\mu$ -tuned CML (Figure 1). Primary and disaggregated SCKs were too small to quantify retention via our optical system. XDLVO calculations under primary conditions predicted an energy barrier to attachment to silica of approximately 180 kT for CML and 23 kT for SCKs (Figure 3b,d solid lines), with repulsive primary minima for CML and attractive primary minima depth exceeding several tens of kT for SCKs. Tuning to the  $n-\mu$  size range decreased the energy barrier height by approximately half and deepened their primary minima for both colloids (Figure 3b,d solid lines). Repulsion decreased despite increased colloid size due to the increased IS. Disaggregation further decreased the energy barriers to attachment to approximately 55 kT (CML) and 5 kT (SCKs) (Figure 3b,d solid lines). That repulsion decreased along with decreased ionic strength was due to simultaneous reduction in colloid size.

Role of Nanoscale Heterogeneity in Retention of  $n-\mu$ -Tuned Colloids. The  $n-\mu$ -tuned colloids experienced substantially lower retention relative to their primary precursors (Figure 1, squares versus triangles) despite their reduced barriers to attachment and deepened primary minima (Figure 3). This nonintuitive result reflects the influence of nanoscale heterogeneity on the kinetics of their attachment

under unfavorable conditions. Whereas attachment for a givensized colloid under unfavorable conditions qualitatively increases with increased IS (reduced repulsive barrier), 42,43 the rate of colloid attachment is also influenced by colloid size.<sup>20</sup> The XDLVO surface interaction profiles described above (Figure 3, solid lines) are mean-field, meaning that they do not reflect nanoscale heterogeneity, since the  $\zeta$ -potentials used in their calculation are insensitive to nanoscale surface heterogeneity. 44 Colloid-surface interaction occurs across a finite zone of interaction (ZOI) that is smaller than the projected area of the colloid, but which scales with the size of the colloid and to the Debye length (inversely to IS).<sup>22</sup> When the ZOI is fully occupied by a heterodomain (nanoscale attractive zone), the energy barrier is eliminated (Figure 3b,d dashed lines). Depending on the relative sizes of ZOIs and heterodomains (as governed by colloid size, heterodomain size, IS, and colloid trajectory), the surface interaction profile will lie between the mean-field (solid lines) and favorable (dashed lines) limits shown in Figure 3. Accordingly, slower attachment rates correspond to colloids that require longer residence times to encounter heterodomains, which are those in the  $n-\mu$  size range because of their least combined diffusion, settling, and fluid drag in the near surface fluid domain.<sup>20</sup>

Upscaled Distribution from Source in Porous Media. Macroscale advection-dispersion-attachment simulations predicted the distribution of CML with distance from the source in a system composed of medium-grained sand (0.51 mm grains) with a porosity of 0.35, and an average pore water velocity of 4 m/day (Figure 2a), utilizing the above-described retention values. In porous media, colloids encounter innumerable collectors (grains), with loss compounded for each collector passed;34 this is why direct injection of nanoscale colloids (i.e., primary) yielded high retained concentrations over a narrow ~1 m zone near their source, as shown (approximately) for injection located at 5 m (Figure 2a, red squares). Tuning the  $n-\mu$  size range reduces clogging and facilitates access to more distant zones, as shown by reduced retention during transport through non-target media, wherein aqueous colloid concentrations decreased by less than a factor of 2 across the 5 m transport distance from the source  $(C = 1.0 \times 10^{11} \text{ CML/L})$  to the end of the non-target zone (C =  $6.3 \times 10^{10}$  CML/L) (Figure 2, blue squares). Despite the reduced concentration upon reaching the target zone (5 m), disaggregation yielded more than 3 orders of magnitude greater retention (10<sup>13.8</sup> versus 10<sup>10.4</sup>) relative to without disaggregation (Figure 2, red versus blue squares), and more than 2 orders of magnitude greater retention relative to the source at 0 m (10<sup>13.8</sup> versus 10<sup>11.2</sup>) (Figure 2). Whereas these number-based concentrations partly reflect the impact of separating aggregates (approximately four primary per aggregate), they mainly reflect the order of magnitude greater experimentally observed retention of nanoscale primary CML relative to the  $n-\mu$ -tuned CML (Figure 1).

Contrasts to Existing Strategies for Nanomaterial **Delivery.** Our proposed targeted delivery strategy contrasts to the Ca<sup>2+</sup>-forced destabilization (aggregation) of HA-FeO<sub>x</sub> NPs<sup>5</sup> in two important ways: (1) disaggregation to the nanoscale size at the target will enhance penetration into the target media and (2) disaggregation at the target can be expected to yield enhanced reactivity because of increased surface area. In addition to reducing their retention on porous media, the reduced diffusion of  $n-\mu$  transition colloids can be expected to limit their mass transfer into matrix porosity (e.g.,

Hunt and Johnson<sup>45</sup>), and thereby facilitate transport through non-target media. Because groundwater generally contains divalent cations (e.g., Ca2+ and Mg2+), inhibition of disaggregation via cation bridging is a potential concern. However, our experiments demonstrated disaggregation of Mg<sup>2+</sup>-aggregated CML and SCKs via simple dilution (Figure 2b,c). If needed, cation bridging can be further mitigated by addition of chelating agents (e.g., ethylenediaminetetraacetic acid, EDTA) $^{46-48}$  to the leading solution.

Since colloid specific densities ranging from 1.0 to 2.6 are demonstrated to display maximal mobility in the  $n-\mu$ transition size range under favorable conditions, 19,20,49 our strategy applies to other carbonaceous materials such as activated carbon and biochar for which specific densities range up to 2.6, and where both types of materials are injected into groundwater for in situ remediation. 13-17 For denser nanoparticles, e.g., FeO<sub>x</sub> NPs (goethite specific density ~4.3), the maximum mobile size range dictated by physical transport (repulsive barrier absent) lies between 50 and 250 nm (radius) (Figure S7). For the sake of demonstration, applying the  $\alpha$ values for CML to the  $\eta$  values for FeO, NPs (since FeO, are stabilized via negatively charged moieties) expands the range of maximal mobility (repulsive barrier present) to smaller sizes (e.g., several tens of nanometers) (Figure S7). Applicability of the proposed delivery strategy will depend not only on colloid density but also on colloid surface properties, and possibly shape. Our work is a substantiated invitation for practitioners to explore implementation of size tuning in order to optimize colloid delivery in target zones of subsurface media.

Executable codes used in this work are available at http:// www.wpjohnsongroup.utah.edu > Research > Downloads.

# ASSOCIATED CONTENT

## Supporting Information

The Supporting Information is available free of charge on the ACS Publications website at DOI: 10.1021/acs.estlett.9b00474.

Materials and methods,  $\zeta$ -potential and colloid size characterization data, time-tracked number-based DLS hydrodynamic radius distribution, disaggregation kinetics, schematic of the impinging jet flow cell, van der Waals equations for layered systems, Hamaker constants and geometric functions, Lewis acid-base and steric energy interactions, XDLVO energies description, parameters utilized in particle trajectory simulations, and synthesis of SCK nanoparticles (PDF)

# AUTHOR INFORMATION

#### **Corresponding Author**

\*Email: william.johnson@utah.edu. Tel: +1 801 585 5033. Fax: +1 801 581 7065.

Mei Dong: 0000-0002-9862-0296

William P. Johnson: 0000-0003-3126-3877

The authors declare no competing financial interest.

# **ACKNOWLEDGMENTS**

This article is based upon work supported by the National Science Foundation Program under grant numbers DMREF-1629078 and DMREF-1629094. Any opinions, findings, and conclusions expressed in this material are those of the authors and do not necessarily reflect the views of the National Science Foundation. We also acknowledge the technical and facility support provided at the Center for High Performance Computing (CHPC) at the University of Utah.

#### REFERENCES

- (1) Elliott, D. W.; Zhang, W. X. Field Assessment of Nanoscale Bimetallic Particles for Groundwater Treatment. *Environ. Sci. Technol.* **2001**, 35, 4922–4926.
- (2) Wood, J. A.; Rehmann, L. Geometric Effects on Non-DLVO Forces: Relevance for Nanosystems. *Langmuir* **2014**, *30*, 4623–4632.
- (3) Fu, F.; Dionysiou, D. D.; Liu, H. The Use of Zero-Valent Iron for Groundwater Remediation and Wastewater Treatment: A Review. *J. Hazard. Mater.* **2014**, *267*, 194–205.
- (4) Cundy, A. B.; Hopkinson, L.; Whitby, R. L. D. Use of Iron-Based Technologies in Contaminated Land and Groundwater Remediation: A Review. *Sci. Total Environ.* **2008**, *400*, 42–51.
- (5) Bianco, C.; Patiño Higuita, J. E.; Tosco, T.; Tiraferri, A.; Sethi, R. Controlled Deposition of Particles in Porous Media for Effective Aquifer Nanoremediation. *Sci. Rep.* **2017**, *7*, 12992.
- (6) McKay, L. D.; Gillham, R. W.; Cherry, J. A. Field Experiments in a Fractured Clay till: 2. Solute and Colloid Transport. *Water Resour. Res.* 1993, 29, 3879–3890.
- (7) Grolimund, D.; Elimelech, M.; Borkovec, M.; Barmettler, K.; Kretzschmar, R.; Sticher, H. Transport of in Situ Mobilized Colloidal Particles in Packed Soil Columns. *Environ. Sci. Technol.* **1998**, 32, 3562–3569.
- (8) Ginn, T. R. A. Travel Time Approach to Exclusion on Transport in Porous Media. *Water Resour. Res.* **2002**, *38*, 12-1–12-11.
- (9) Keller, A. A.; Sirivithayapakorn, S.; Chrysikopoulos, C. V. Early Breakthrough of Colloids and Bacteriophage MS2 in a Water-Saturated Sand Column. *Water Resour. Res.* **2004**, *40*, 1–11.
- (10) Vasiliadou, I. A.; Chrysikopoulos, C. V. Cotransport of Pseudomonas Putida and Kaolinite Particles through Water-Saturated Columns Packed with Glass Beads. *Water Resour. Res.* **2011**, 47, WO2543
- (11) Chrysikopoulos, C. V.; Katzourakis, V. E. Colloid Particle Size-Dependent Dispersivity. *Water Resour. Res.* **2015**, *51*, 4668–4683.
- (12) Zhang, P.; Johnson, W. P.; Piana, M. J.; Fuller, C. C.; Naftz, D. L. Potential Artifacts in Interpretation of Differential Breakthrough of Colloids and Dissolved Tracers in the Context of Transport in a Zero-Valent Iron Permeable Reactive Barrier. *Groundwater* **2001**, *39*, 831–840
- (13) Busch, J.; Meißner, T.; Potthoff, A.; Bleyl, S.; Georgi, A.; Mackenzie, K.; Trabitzsch, R.; Werban, U.; Oswald, S. E. A Field Investigation on Transport of Carbon-Supported Nanoscale Zero-Valent Iron (NZVI) in Groundwater. J. Contam. Hydrol. 2015, 181, 59–68.
- (14) Gomez-Eyles, J. L.; Yupanqui, C.; Beckingham, B.; Riedel, G.; Gilmour, C.; Ghosh, U. Evaluation of Biochars and Activated Carbons for in Situ Remediation of Sediments Impacted with Organics, Mercury, and Methylmercury. *Environ. Sci. Technol.* **2013**, *47*, 13721–13729
- (15) Jahan, S.; Alias, Y. B.; Bakar, A. F. B. A.; Yusoff, I. Bin Transport and Retention Behavior of Carbonaceous Colloids in Natural Aqueous Medium: Impact of Water Chemistry. *Chemosphere* **2019**, 217, 213–222.
- (16) Rakowska, M. I.; Kupryianchyk, D.; Harmsen, J.; Grotenhuis, T.; Koelmans, A. A. In Situ Remediation of Contaminated Sediments Using Carbonaceous Materials. *Environ. Toxicol. Chem.* **2012**, *31*, 693–704.
- (17) Song, B.; Zeng, G.; Gong, J.; Liang, J.; Xu, P.; Liu, Z.; Zhang, Y.; Zhang, C.; Cheng, M.; Liu, Y.; Ye, S.; Yi, H.; Ren, X. Evaluation Methods for Assessing Effectiveness of in Situ Remediation of Soil and Sediment Contaminated with Organic Pollutants and Heavy Metals. *Environ. Int.* **2017**, *105*, 43–55.

- (18) Rajagopalan, R.; Tien, C. Trajectory Analysis of Deep-bed Filtration with the Sphere-in-cell Porous Media Model. *AIChE J.* **1976**, 22, 523–533.
- (19) Yao, K.; Habibian, M. T.; O'Melia, C. R. Water and Waste Water Filtration: Concepts and Applications. *Environ. Sci. Technol.* **1971**, *5*, 1105–1112.
- (20) Ron, C. A.; VanNess, K.; Rasmuson, A.; Johnson, W. P. How Nanoscale Surface Heterogeneity Impacts Transport of Nanoto Micro-Particles on Surfaces under Unfavorable Attachment Conditions. *Environ. Sci.: Nano* **2019**. *6*. 1921–1931.
- (21) Molnar, I. L.; Johnson, W. P.; Gerhard, J. I.; Willson, C. S.; O'Carroll, D. M. Predicting Colloid Transport through Saturated Porous Media: A Critical Review. *Water Resour. Res.* **2015**, *51*, 6804–6845.
- (22) Duffadar, R.; Kalasin, S.; Davis, J. M.; Santore, M. M. The Impact of Nanoscale Chemical Features on Micron-Scale Adhesion: Crossover from Heterogeneity-Dominated to Mean-Field Behavior. *J. Colloid Interface Sci.* **2009**, 337, 396–407.
- (23) Kozlova, N.; Santore, M. M. Manipulation of Micrometer-Scale Adhesion by Tuning Nanometer-Scale Surface Features. *Langmuir* **2006**, 22, 1135–1142.
- (24) Pazmino, E.; Trauscht, J.; Dame, B.; Johnson, W. P. Power Law Size-Distributed Heterogeneity Explains Colloid Retention on Soda Lime Glass in the Presence of Energy Barriers. *Langmuir* **2014**, *30*, 5412–5421.
- (25) Rasmuson, A.; Pazmino, E.; Assemi, S.; Johnson, W. P. Contribution of Nano- to Microscale Roughness to Heterogeneity: Closing the Gap between Unfavorable and Favorable Colloid Attachment Conditions. *Environ. Sci. Technol.* **2017**, *51*, 2151–2160.
- (26) Rasmuson, A.; VanNess, K.; Ron, C. A.; Johnson, W. P. Hydrodynamic versus Surface Interaction Impacts of Roughness in Closing the Gap between Favorable and Unfavorable Colloid Transport Conditions. *Environ. Sci. Technol.* **2019**, *53*, 2450–2459.
- (27) Shen, C.; Jin, Y.; Zhuang, J.; Li, T.; Xing, B. Role and Importance of Surface Heterogeneities in Transport of Particles in Saturated Porous Media. *Crit. Rev. Environ. Sci. Technol.* **2019**, 1–86. (28) Elimelech, M.; O'Melia, C. R. Kinetics of Deposition of Colloidal Particles in Porous Media. *Environ. Sci. Technol.* **1990**, 24,
- (29) Flores, J. A.; Pavía-Sanders, A.; Chen, Y.; Pochan, D. J.; Wooley, K. L. Recyclable Hybrid Inorganic/Organic Magnetically Active Networks for the Sequestration of Crude Oil from Aqueous Environments. *Chem. Mater.* **2015**, 27, 3775–3782.
- (30) Trauscht, J.; Pazmino, E.; Johnson, W. P. Prediction of Nanoparticle and Colloid Attachment on Unfavorable Mineral Surfaces Using Representative Discrete Heterogeneity. *Langmuir* **2015**, *31*, 9366–9378.
- (31) Ma, H.; Pazmino, E.; Johnson, W. P. Surface Heterogeneity on Hemispheres-in-Cell Model Yields All Experimentally-Observed Non-Straining Colloid Retention Mechanisms in Porous Media in the Presence of Energy Barriers. *Langmuir* **2011**, *27*, 14982–14994.
- (32) VanNess, K.; Rasmuson, A.; Ron, C. A.; Johnson, W. P. A Unified Force and Torque Balance for Colloid Transport: Predicting Attachment and Mobilization under Favorable and Unfavorable Conditions. *Langmuir* **2019**, *35*, 9061–9070.
- (33) Happel, J. Viscous Flow in Multiparticle Systems: Slow Motion of Fluids Relative to Beds of Spherical Particles. *AIChE J.* **1958**, *4*, 197–201.
- (34) Johnson, W. P.; Hilpert, M. Upscaling Colloid Transport and Retention under Unfavorable Conditions: Linking Mass Transfer to Pore and Grain Topology. *Water Resour. Res.* **2013**, *49*, 5328–5341.
- (35) Johnson, W. P.; Rasmuson, A.; Pazmiño, E.; Hilpert, M. Why Variant Colloid Transport Behaviors Emerge among Identical Individuals in Porous Media When Colloid—Surface Repulsion Exists. *Environ. Sci. Technol.* **2018**, *52*, 7230—7239.
- (36) Bedrikovetsky, P.; Osipov, Y.; Kuzmina, L.; Malgaresi, G. Exact Upscaling for Transport of Size-Distributed Colloids. *Water Resour. Res.* **2019**, *55*, 1011–1039.

1528-1536.

- (37) Tong, M.; Johnson, W. P. Excess Colloid Retention in Porous Media as a Function of Colloid Size, Fluid Velocity, and Grain Angularity. *Environ. Sci. Technol.* **2006**, *40*, 7725–7731.
- (38) Huynh, K. A.; Chen, K. L. Aggregation Kinetics of Citrate and Polyvinylpyrrolidone Coated Silver Nanoparticles in Monovalent and Divalent Electrolyte Solutions. *Environ. Sci. Technol.* **2011**, *45*, 5564–5571.
- (39) Akaighe, N.; Depner, S. W.; Banerjee, S.; Sharma, V. K.; Sohn, M. The Effects of Monovalent and Divalent Cations on the Stability of Silver Nanoparticles Formed from Direct Reduction of Silver Ions by Suwannee River Humic Acid/Natural Organic Matter. *Sci. Total Environ.* **2012**, 441, 277–289.
- (40) Baalousha, M.; Nur, Y.; Römer, I.; Tejamaya, M.; Lead, J. R. Effect of Monovalent and Divalent Cations, Anions and Fulvic Acid on Aggregation of Citrate-Coated Silver Nanoparticles. *Sci. Total Environ.* **2013**, 454–455, 119–131.
- (41) Shen, C.; Wu, L.; Zhang, S.; Ye, H.; Li, B.; Huang, Y. Heteroaggregation of Microparticles with Nanoparticles Changes the Chemical Reversibility of the Microparticles' Attachment to Planar Surfaces. *J. Colloid Interface Sci.* **2014**, *421*, 103–113.
- (42) Tufenkji, N.; Elimelech, M. Deviation from the Classical Colloid Filtration Theory in the Presence of Repulsive DLVO Interactions. *Langmuir* **2004**, *20*, 10818–10828.
- (43) Johnson, W. P.; Tong, M. Observed and Simulated Fluid Drag Effects on Colloid Deposition in the Presence of an Energy Barrier in an Impinging Jet System. *Environ. Sci. Technol.* **2006**, *40*, 5015–5021.
- (44) Elimelech, M.; Nagai, M.; Ko, C. H.; Ryan, J. N. Relative Insignificance of Mineral Grain Zeta Potential to Colloid Transport in Geochemically Heterogeneous Porous Media. *Environ. Sci. Technol.* **2000**, 34, 2143–2148.
- (45) Hunt, R. J.; Johnson, W. P. Pathogen Transport in Groundwater Systems: Contrasts with Traditional Solute Transport. *Hydrogeol. J.* **2017**, *25*, 921–930.
- (46) Armstrong, P. B.; Jones, D. P. On the Role of Metal Cations in Cellular Adhesion: Cation Specificity. *J. Exp. Zool.* **1968**, *167*, 275–282.
- (47) Morris, S. J.; Chiu, V. C. K.; Haynes, D. H. Divalent Cation-Induced Aggregation of Chromaffin Granule Membranes. *Membr. Biochem.* 1979, 2, 163–201.
- (48) Liao, B. Q.; Allen, D. G.; Leppard, G. G.; Droppo, I. G.; Liss, S. N. Interparticle Interactions Affecting the Stability of Sludge Flocs. *J. Colloid Interface Sci.* **2002**, 249, 372–380.
- (49) Elimelech, M.; Gregory, J.; Jia, X.; Williams, R. A. Particle Deposition and Aggregation; Butterworth-Heinemann: Woburn, MA, USA, 1995.